Evaluation of Absorption and Emission Properties of Yb^{3+} Doped Crystals for Laser Applications

Laura D. DeLoach, Stephen A. Payne, L. L. Chase, Larry K. Smith, Wayne L. Kway, and William F. Krupke

Abstract—**The emission and absorption properties of numerous host crystals doped with Yb^{3+} ions have been studied. The hosts which have been selected present a variety of crystal field environments for the ytterbium ion, including fluoride and oxide crystals with six-, seven-, eight-, nine- and twelvefold coordinated substitutional sites. The crystal compounds include $LiYF_4$, LaF_3, SrF_2, BaF_2, $KCaF_3$, KY_3F_{10}, Rb_2NaYF_6, BaY_2F_8, Y_2SiO_5, $Y_3Al_5O_{12}$, $YAlO_3$, $LuPO_4$, $Ca_5(PO_4)_3F$, $LiYO_2$, and $ScBO_3$. Spectral determinations have been made of the resonant absorption and emission cross sections between 850 and 1100 nm, and the emission decay times of the upper laser level have been measured. The emission cross sections have been evaluated using the absorption cross section and principle of reciprocity, and again using the Füchtbauer–Ladenburg formula. Agreement between the two methods is within 20% for most materials. The results of this survey are discussed in the framework of requirements for an effective diode-pumped Yb^{3+} laser system. $Ca_5(PO_4)_3F$: Yb is predicted to exhibit the most useful laser properties and is expected to be superior to $Y_3Al_5O_{12}$: Yb in many key spectroscopic parameter values.**

I. Introduction

DIODE lasers offer many desirable properties for laser-pumped laser applications. They are compact, efficient, may be wavelength tuned to match a particular pump transition, and have a highly directed and focusable output. Consequently, it is possible to exceed pumping efficiencies of 90% with diode lasers. Moreover, high peak optical densities of the pump transition will result in smaller laser elements and more compact designs than are possible with flashlamp pumping. Selective diode pumping also leads to reduced heating of the laser medium due to the lower quantum defect between the pump and laser photon energies, thereby minimizing thermal lensing and the possibility of catastrophic fracture. Additionally, diode lasers are reliable pump sources, with long operating lifetimes. These properties and a progressively decreasing price of pump power contribute to the overall attractiveness of diode laser pump sources.

Recent advances in high performance strained layer diode lasers with wavelengths between 0.9 and 1.1 μm have stimulated interest in diode pumped Yb^{3+} lasers [1], [2]. The ytterbium ion is ideally suited for diode-pumping since it has a very simple energy level scheme with desirable properties for a laser system. Yb^{3+} has a $4f^{13}$ shell which lacks one electron compared to a filled shell. There are only two manifolds, the ground $^2F_{7/2}$ state and an excited $^2F_{5/2}$ state, which are separated by approximately 10 000 cm^{-1}. Since only a single spectral band is available for pumping energy into the system, the previous use of the white light from flashlamps rendered Yb impractical as a laser ion [3]. Reinberg *et al.* were the first to employ a narrow band source to pump Yb ions. In this early work, they used an incoherent Si:GaAs diode to pump Yb:YAG at low temperature [4]. The recent introduction of InGaAs laser diodes allowed the effective coupling of pump light into the gain medium, so as to permit the efficient room temperature operation of Yb:YAG [5]. Furthermore, because there are no additional $4f$ energy levels, as in other trivalent rare earths, complications in laser media which result from concentration quenching, upconversion and excited state absorption are not anticipated to affect laser performance. Most other laser ions such as Nd^{3+} and Er^{3+}, do encounter some detrimental impact and design limitations from these effects.

Recent calculations by Krupke and Chase [6] have suggested that InGaAs-pumped Yb:YAG (Yb^{3+} in $Y_3Al_5O_{12}$) might serve usefully as an energy-storing laser system. Subsequent work by T. Y. Fan and co-workers [5] involved the demonstration of an efficient InGaAs diode-pumped Yb:YAG oscillator. The purpose of the paper reported here is to survey the optical properties of numerous crystals doped with Yb^{3+} in order to assess their potential laser performance in diode pumped systems and to identify Yb-gain media potentially superior to Yb:YAG. Our interest is twofold: to study and understand the energy levels and special features of the ytterbium ion in various crystal field environments, and also to identify specific candidates for laser operation.

This paper reports absorption and emission cross sections of the $^2F_{7/2}$–$^2F_{5/2}$ transition, and the upper laser level lifetimes of the Yb^{3+} ion for numerous oxide and fluoride crystals. The experimental procedures are described for the absorption and emission spectroscopy and the measured emission lifetimes in Section II. The emission cross sections have been evaluated using the method of reciprocity and the Füchtbauer–Ladenburg formula and are

Manuscript received July 6, 1992. This work was performed under the auspices of the U.S. Department of Energy by Lawrence Livermore National Laboratory under contract W-7405-ENG-48.

The authors are with the Lawrence Livermore National Laboratory, University of California, Livermore, CA 94550.

IEEE Log Number 9207473.

TABLE I
Yb^{3+} DOPED CRYSTALS USED IN THIS PAPER
(ZM = zone-melting; CZ = Czochralski; BM = Bridgman; D = distorted version of structure type; LLNL = Lawrence Livermore National Laboratory; ORNL = Oak Ridge National Laboratory)

Host	Concentration ($10^{20}Yb^{3+}/cm^3$)	Density (g/cm^3)	Source	Growth Method	Optical Class	Crystal Structure Type	Substitutional Site, Coord. No.
$LiYF_4$ (YLF)	1.44	3.77	Sanders	CZ	Uniaxial	Scheelite	Y,8
LaF_3	0.22	5.94	LLNL	ZM	Uniaxial	Tysonite	La,9
SrF_2	0.10	4.24	Optovac	BM	Isotropic	Fluorite	Sr,8
BaF_2	0.16	4.83	Optovac	BM	Isotropic	Fluorite	Ba,8
$KCaF_3$	1.40	2.67	LLNL	BM	Biaxial	Perovskite (D)	Ca,6
KY_3F_{10}	1.45	4.31	LLNL	ZM	Isotropic	—	Y,8
Rb_2NaYF_6	1.03	~3.4	LLNL	ZM	Isotropic	Elpasolite	Y,6
BaY_2F_8	1.40	4.97	LLNL	ZM	Biaxial	—	Y,8
Y_2SiO_5 (YOS)	1.83	4.44	LLNL	CZ	Biaxial	—	Y,6
$Y_3Al_5O_{12}$ (YAG)	1.36	4.55	LLNL	CZ	Isotropic	Garnet	Y,8
$YAlO_3$ (YALO)	6.82	5.35	LLNL	CZ	Biaxial	Perovskite (D)	Y,12
$Ca_5(PO_4)_3F$ (FAP)	0.36	3.19	LLNL	CZ	Uniaxial	Apatite	Ca_{II},7
$LuPO_4$	0.80	5.53	ORNL	Flux	Uniaxial	Zircon	Lu,8
$LiYO_2$	2.27	4.12	LLNL	CZ	Biaxial	Rock salt (D)	Y,6
$ScBO_3$	1.32	3.45	LLNL	CZ	Uniaxial	Calcite	Sc,6

both discussed in Section III. The results of our measurements are presented in Section IV. Section V contains an analysis and summary of the relevant properties of Yb, and our conclusions are stated in Section VI.

II. EXPERIMENTAL METHODS

A. Crystal Samples

Fifteen samples of different oxide and fluoride crystals doped with Yb^{3+} were obtained from a variety of sources. Table I lists optical class, measured Yb^{3+} concentration, density, source from which each was obtained, growth method, crystal structure type, and the coordination number of the rare earth substitutional site. Additional samples of BaF_2 and SrF_2 doped with different Yb^{3+} concentrations were also examined. The samples reported are those for which the Yb^{3+} existed in an unclustered site environment. The ytterbium concentrations were determined at Lawrence Livermore National Laboratory (LLNL) by inductively coupled plasma (ICP) atomic emission spectrometry or by ICP mass spectrometry.

B. Conventional Spectroscopy

All of the data reported herein were obtained at room temperature. A Perkin–Elmer Lambda 9 Spectrophotometer and commercial software package were employed for acquisition of the absorption spectra. Polarized absorption spectra were obtained in the cases of optically anisotropic crystals from samples large enough to be fabricated into cubes oriented along their dielectric axes.

The emission spectra were acquired by exciting the oriented sample with a Nd : YAG laser-pumped dye laser using the LDS-698 dye. The LDS-698 laser light in turn was converted to the 1 μm region by way of a H_2 Raman shift cell. The sample emission was dispersed with a grating monochromator blazed at 1 μm, and an S-1 photomultiplier tube was positioned to detect the signal. A standard lamp was utilized to determine the sensitivity of the monochromator/detector combination and all spectra were corrected accordingly. The data acquisition was accomplished with the help of an IBM computer model PS2. A Stanford Research Systems boxcar/interface system was controlled using software developed in our laboratory.

Lifetimes of the Yb^{3+} ions were measured by utilizing the same detector and source described for the emission measurements. The monochromator was set to monitor the emission at discrete wavelengths between 950 and 1050 nm. A Nicolet LAS 12/70 transient digitizer accumulated and averaged the electrical output of the S-1 PMT after it passed through a discriminator. Data were transferred and handled numerically by a desktop Hewlett Packard computer. The reported lifetimes are the best fit exponentials.

III. EMISSION CROSS SECTIONS

The emission cross sections are determined using either the method of reciprocity (RM), or the Füchtbauer–Ladenburg (F–L) formula, and we have carried out both determinations where sufficient information is available. The cross section obtained by reciprocity requires absolute polarized absorption cross sections and detailed knowledge of the system's energy levels and degeneracies. The input parameters for the F–L formula are the emission line shape function, the radiative lifetime and the refractive index. Whenever possible, both methods are employed to independently check the accuracy of the measurements. The theoretical details concerning the cross section determinations are discussed in subsections A, B, and C. Part D of this section contains a brief description of the absorption and emission properties desired of the diode-pumped Yb-laser material.

A. The Method of Reciprocity

The basis for reciprocity [6]–[8] may be described by writing the emission and absorption cross sections in terms of the energy levels E_k and degeneracies d_k. The sum-

mation of the individual cross section σ_{ij} between the ith and jth lower and upper energy levels can be formulated to describe both the absorption and emission cross sections:

$$\sigma_{em}(\nu) = \sum_{ij} d_j \frac{3\exp(-E_j/kT)}{Z_u} \sigma_{ji}(\nu)\, d_i \quad (1)$$

$$\sigma_{abs}(\nu) = \sum_{ij} d_i \frac{\exp(-E_i/kT)}{Z_l} \sigma_{ij}(\nu)\, d_j \quad (2)$$

where Z, the partition function, is defined as

$$Z_k = \sum_k d_k \exp(-E_k/kT). \quad (3)$$

The partition functions are simply equal to the degeneracies of the two states at high temperature. The $\sigma(\nu)$ functions contain line shape information. In each case, the energies E and the partition functions Z are measured from the lowest crystal field level of the $^2F_{7/2}$, (l), and the $^2F_{5/2}$, (u), electronic states.

The use of reciprocity, $\sigma_{ij} = \sigma_{ji}$, and the division of (1) by (2) is used to obtain an emission cross section in terms of the absorption cross section. It will also be helpful to first define an energy parameter, the zero-line energy, E_{ZL}, to be the energy separation between the lowest components of the upper and lower crystal field states. Thus, a particular energy separation may be written as:

$$E_j - E_i = h\nu - E_{ZL} \quad (4)$$

Now, the emission cross section is readily formulated from the absorption cross section with energy level parameters, E_{ZL}, Z_l, and Z_u as follows:

$$\sigma_{em}(\nu) = \sigma_{abs}(\nu) \frac{Z_l}{Z_u} \exp[(E_{ZL} - h\nu)/kT]. \quad (5)$$

The reciprocity method may be employed for those materials with appropriately detailed energy level data. The energy level determinations extracted from the literature, which were generally made at low temperatures, are combined with our spectral measurements which have been obtained at room temperature. This temperature difference should have only a negligible effect on our results, however. Interestingly, the line shape function is simply *multiplied* by the ratio of the partition functions Z_l/Z_u and the exponential function containing the zero-line energy, $\exp(E_{ZL}/kT)$, and consequently, does not influence the spectral shape, but only the *magnitude*, or scaling, of the cross section. The absorption line shape is transformed to that of the emission solely on the basis of the $\exp(-h\nu/kT)$ term.

B. Füchtbauer–Ladenburg Equation

The fundamental relationship between spontaneous and stimulated emission rates embodied in the Füchtbauer–Ladenburg (F–L) equation allows a straightforward calculation of the emission cross section using input parameters which are readily attained. The form of the equation is [9]:

$$\sigma^{\alpha}_{em}(\nu) = \frac{\lambda^2 g^{\alpha}(\nu)}{8\pi n^2 \tau_{rad}}. \quad (6)$$

Here, n is the refractive index, τ_{rad} is the radiative lifetime, and $g(\nu)$, the normalized line shape function for polarization α in units of photons per second, is

$$g^{\alpha}(\nu) = \frac{3S_{\alpha}}{\sum_{\beta} S_{\beta}}. \quad (7)$$

The three polarized emission spectra are summed in the denominator (for the anisotropic crystals). The corrected emission spectra S_{α}, in photons/s have been determined for the Yb-doped crystals discussed in this paper. Although the emission decay times τ_{em} have also been measured as described in Section II, the actual radiative lifetime τ_{rad} may potentially be different as a result of quenching by impurities and effects of clustering in the case of charge compensated samples. Where no additional information is available $\tau_{rad} = \tau_{em}$ was utilized.

C. Corroboration of Emission Lifetimes

For several samples, both the cross section determined by the RM and the cross section calculated by the F–L equation are available. Our means of corroborating the emission lifetimes is displayed in Fig. 1, using Yb:YAG as an example. First, the absorption spectrum (σ_{abs}) is converted into a "calculated" emission spectrum σ^{calc}_{em} by way of the RM (part A). The F–L method is then employed to obtain a completely independent assessment of the emission cross section, using the "measured" emission spectrum $g(\nu)$ and lifetime τ_{em}. Now, it is possible to independently check the measured lifetime τ_{em} against a calculated value of τ_{rad} obtained using the results from the two cross section evaluations. For this procedure, we set σ^{calc}_{em} equal to σ^{meas}_{em} and solve for the τ_{rad} value which gives the best agreement overall, see part C of Fig. 1. (The procedure is straight-forward in cubic crystals for which only a single unpolarized spectrum is required. Anisotropic crystals, however, require several polarized spectra in order to determine the value of τ_{rad} that accounts for all of the polarizations.) The agreement typically obtained between the measured emission decay time τ_{em} and the calculated radiative lifetime τ_{rad} is within 20% for cases in which all of the necessary information is available, see parts D and E of the figure.

D. Energy Extraction from Diode-Pumped Systems

We are interested in the potential performance of a diode-pumped Yb laser. Thus, both emission and absorption properties of the Yb^{3+} ion must be evaluated to determine if the material can adequately perform in this designated application. An accurate measure of the emission cross section is needed to assess the emission saturation fluence F_{ext} at the extraction wavelength λ_{ext} [10]

$$F_{ext} = hc/\sigma_{ext}\lambda_{ext}. \quad (8)$$

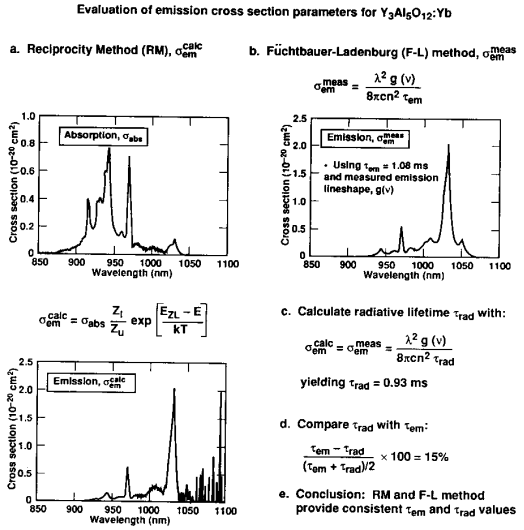

Fig. 1. The determination of emission cross sections and the corroboration of emission lifetimes are outlined using $Y_3Al_5O_{12}$:Yb (YAG:Yb) as an example. a) Using the equation for reciprocity, the absorption cross section σ_{abs} for YAG:Yb is converted to a "calculated" emission cross section σ_{em}^{calc}. b) Using the Füchtbauer-Ladenburg equation, the "measured" emission cross section σ_{em}^{meas} of YAG:Yb is obtained from the experimentally obtained emission spectra $g(\nu)$ and emission decay time τ_{em}. c) The radiative lifetime τ_{rad} is obtained by matching the calculated and measured emission cross sections and solving for τ_{rad} in the Füchtbauer–Ladenburg equation. d) The comparison of τ_{rad} and τ_{em} reveals consistent values within 15% for YAG:Yb.

Here, σ_{ext} is the value of the emission cross section (σ_{em}) at the chosen extraction wavelength. Smaller values of F_{ext} allow for simpler means of extraction for the case of a laser amplifier, and also lead to a lower threshold for a CW oscillator type configuration. The actual magnitude of σ_{ext} which is most useful will depend on the pulse length, pumping conditions, the damage threshold of the optical components and other factors. For nanosecond timescale pulse lengths, emission cross sections in the range of $\sigma_{ext} > 10^{-20}$ cm^2 are generally required.

The extraction efficiency and laser threshold of Yb-doped materials are also strongly impacted by the presence of ground state resonance absorption at the laser wavelength. All Yb lasers are expected to be quasi-four-level systems. Thus, it is first recognized that the maximum fraction of the stored energy that can be extracted under the most desirable conditions (where all the Yb ions are pumped to the excited state and the fluence of the extraction beam is much larger than F_{ext}), is given by

$$f_{max}(\lambda) = \frac{\sigma_{ext}(\lambda_{ext})}{\sigma_{ext}(\lambda_{ext}) + \sigma_{abs}(\lambda_{ext})}. \quad (9)$$

Essentially, the laser field reaches equilibrium with the material, and the upward and downward transition rates become equal as the magnitude of f_{max} is approached. Using (5), (9) can be rewritten as

$$f_{max}(\lambda) = \left\{1 + \frac{Z_u}{Z_l} \exp\left[(hc/\lambda - E_{ZL})/kT\right]\right\}^{-1}. \quad (10)$$

The energy difference ΔE between the photon energy and E_{ZL} is primarily determined by the energy of the terminal level above the ground state. If we take the partition function ratio Z_u/Z_l to be roughly unity, we can estimate that the extraction efficiencies F_{max} will be 0.50, 0.73, 0.88, and 0.95 for $\Delta E = (E_{ZL} - hc/\lambda)$ values of 0, 205, 410, and 615 cm^{-1}, respectively, (kT at room temperature is 205 cm^{-1}). The more useful Yb laser materials operating in a short-pulse extraction mode, will therefore require $\Delta E > 400$ cm^{-1}. In other words, the system will operate most efficiently if the extraction occurs at the longest feasible wavelength that remains consistent with an adequate emission cross section.

For all configurations of efficient diode-pumped Yb-laser systems, it will be necessary to drive a substantial fraction of the ground state Yb ions to the excited state, in order to achieve adequate gain (and to overwhelm the ground state absorption losses). The ease with which this ground state depletion may be accomplished depends on the absorption cross section σ_{abs} and the emission lifetime τ_{em}. This is described by the pump saturation intensity parameter:

$$I_{sat} = h\nu/(\sigma_{abs}\tau_{em}). \quad (11)$$

The importance of I_{sat} can be recognized by noting that the fraction of excited Yb ions is given by I_{abs}/I_{sat} in the low doping limit, where I_{abs} is the absorbed pump power. Since InGaAs diode sources are regarded as peak-power-limited devices, clearly a long emission lifetime is favorable in order to accumulate a greater population inversion for a given peak power. We can also calculate the minimum fraction of Yb^{3+} ions that must be excited such that the ground state absorption and the gain exactly balance, and there is net transparency at λ_{ext}. This quantity β_{min} is simply given by [3]

$$\beta_{min} = \frac{\sigma_{abs}(\lambda_{ext})}{\sigma_{ext}(\lambda_{ext}) + \sigma_{abs}(\lambda_{ext})}. \quad (12)$$

Notice that $\beta_{min} = 1 - f_{max}$, as is reasonable, see (9).

For the case of a crystal having low absorption at the pump wavelength, the minimum pump intensity required to achieve transparency at the extraction wavelength is given by

$$I_{min} = \beta_{min} I_{sat} \quad (13)$$

where we have obtained (13) by setting the fraction of excited Yb ions (I_{abs}/I_{sat}) equal to the required fractional excitation of β_{min}, such that $I_{min} = I_{abs}$. I_{min} may be interpreted as the absorbed pump intensity required to reach threshold in an otherwise lossless oscillator, or to have the absorption and gain become exactly equal at the chosen extraction wavelength λ_{ext} in an amplifier configuration. The interdependencies of the key spectroscopic parameters, in relation to the design of strongly pumped rare-earth lasers, has been given for Yb:YAG [6]. A large σ_{abs} permits a lower Yb doping level to be used for the gain element (of a given size). This in turn leads to a lower

resonance absorption loss coefficient and therefore to a higher small-signal gain coefficient for a given pump flux. I_{min} will later be utilized as a figure-of-merit, by which to order the relative usefulness of various Yb-doped media.

In the ensuing sections, the results of our spectroscopic measurements are discussed with attention to their potential usefulness in a diode-pumped Q-switched oscillator or a nanosecond-pulse amplifier configuration.

IV. Results

Samples were selected which allow the study of the Yb^{3+} ion in a variety of crystal field environments in order to characterize the range of spectroscopic properties that are possible. The Yb^{3+} ions occupy sites of true octahedral symmetry in the Rb_2NaYF_6 host, which crystallizes with the elpasolite structure, as noted in Table I. For SrF_2 and BaF_2, which possess the fluorite structure, the cubic eightfold site symmetry is only mildly disrupted by the charge compensation required when trivalent ytterbium replaces the divalent metal ions. $KCaF_3$ is another example of a Yb^{3+} replacing a divalent cation in a cubic site, although here the Ca site is sixfold coordinated for this distorted perovskite structure. Several of the selected crystals exhibit a distorted eightfold coordination, including $LiYF_4$ (scheelite structure), BaY_2F_8, KY_3F_{10}, $Y_3Al_5O_{12}$ (garnet structure), and $LuPO_4$ (zircon structure). Y_2SiO_5 actually has two sixfold coordinated yttrium sites which are nearly identical. The sixfold coordinated site of $ScBO_3$ (calcite structure) is centrosymmetric, while it possesses strong odd parity fields for $LiYO_2$ (distorted rock salt structure). Yb^{3+} in LaF_3 is ninefold coordinated by fluorines, and is twelvefold coordinated in $YAlO_3$ (distorted perovskite structure). The substitutional site in $Ca_5(PO_4)_3F$ (apatite structure) includes both fluorine and oxygen, and involves a highly irregular sevenfold coordinated site.

The measured emission and absorption spectra obtained between 850 and 1100 nm are presented for each material in Figs. 2-4. Each frame in the figures has the polarized absorption and emission spectra plotted on an absolute cross section scale. A single, unpolarized spectrum fully describes optically isotropic crystals, while several polarized spectra measured parallel to the dielectric axes may be required for anisotropic crystals. Two spectra are needed for uniaxial and three spectra are needed for biaxial crystals to characterize the electric-dipole transitions. The resonant transition of Yb^{3+} is, however, also magnetic-dipole allowed. Thus, in order to account fully for the oscillator strength, spectra would have to be acquired for additional orientations. The contribution of the magnetic dipole to the oscillator strength may be significant for some crystals; the calculated magnetic-dipole lifetime of the Yb^{3+} ion, following Carnall *et al.* is approximately 15 ms for a fluoride [11]. We have only observed lifetimes on this order for three crystals: CaF_2, SrF_2, and Rb_2NaYF_6. Now, since all of these crystals are cubic, only a single unpolarized spectrum is required in any case. As a result, we assume that two (three) spectra are sufficient to fully characterize the uniaxial (biaxial) systems, since these crystals are minimally influenced by the magnetic-dipole contribution.

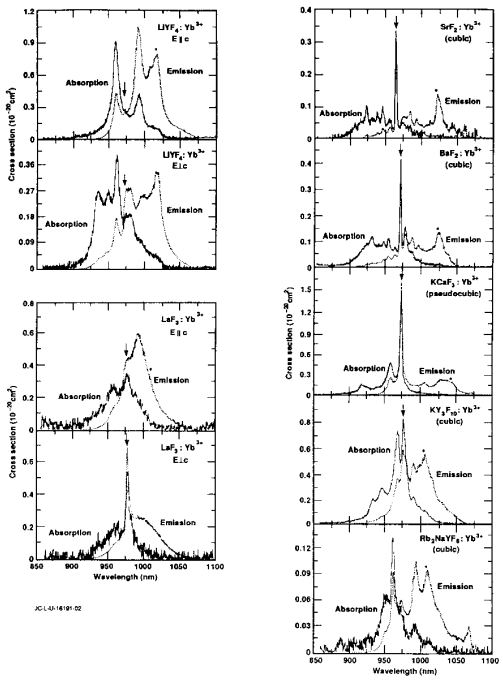

Fig. 2. Room temperature absorption and emission spectra of Yb^{3+} in various fluoride crystal hosts are shown. Data are plotted on an absolute cross section scale. Polarized spectra for noncubic crystals are specifically denoted. In each set of spectra, an arrow is used to designate the wavelength of the zero-line, and an asterisk marks the wavelength selected for the most suitable short-pulse extraction. The difference in photon energy between the wavelengths thusly marked is the value of ΔE. The values of the emission cross section, and the wavelength marked by the asterisks correspond to the σ_{ext} and λ_{ext} in Table III.

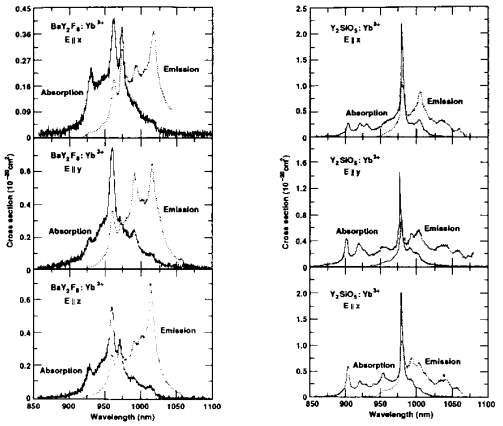

Fig. 3. Room temperature absorption and emission spectra of Yb^{3+} in two biaxial crystal hosts are shown. The polarized spectra along the three principal dielectric axes are noted. An arrow marks the wavelength of the zero-line and an asterisk denotes the wavelength for the most suitable short-pulse extraction. The values corresponding to the relevant parameters are enumerated in Table III.

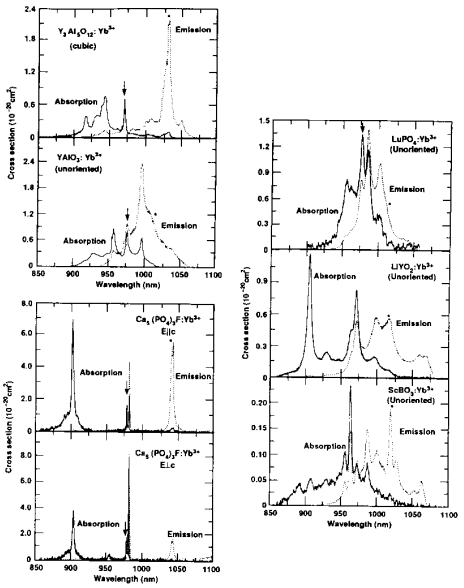

Fig. 4. Room temperature absorption and emission spectra of Yb^{3+} in several oxide crystal hosts are shown. For polarized spectra, orientations are specifically noted. An arrow marks the wavelength of the zero-line and an asterisk denotes the wavelength of the most suitable short-pulse extraction. Corresponding values for σ_{ext}, λ_{ext}, and ΔE are enumerated in Table III.

TABLE II
PARAMETERS FOR σ_{em} CALCULATIONS OF Yb^{3+}-DOPED CRYSTALS
(*est* = estimated; parentheses reflect uncertainty in the value of the quantity)

Host	Zero-Line λ_{ZL}(nm)	Partition Function Ratio, Z_l/Z_u	Refractive Index, n_{ave}	References
$LiYF_4$	972.0	0.88	1.455	[12]
LaF_3	974.7	1.41	1.597	[13]
SrF_2	966.5	(0.97)	1.438	[14,15]
BaF_2	966.7	(0.97)	1.473	[14,15]
$KCaF_3$	(972.0)	(0.73)	1.378	[16]
KY_3F_{10}	974.2	1.24	1.500	[17,18]
Rb_2NaYF_6	(968)	(1.0)	1.403	[19,20]
BaY_2F_8	(972.6)	(1.0)	1.521	[21]
Y_2SiO_5	(979)	(1.0)	1.790	[22]
$Y_3Al_5O_{12}$	968.3	0.80	1.820	[23,24]
$YAlO_3$	978.5	1.09	1.956	[25-27]
$Ca_5(PO_4)_3F$	981.5	1.1	1.630	[28,29]
$LuPO_4$	976.1	0.96	1.83 (est.)	[30]
$LiYO_2$	(972.6)	(1.0)	1.82 (est.)	[31]
$ScBO_3$	(974.6)	(1.0)	1.84	[32]

Several of the parameters which are necessary to calculate the emission cross sections utilizing the F-L equation or the method of reciprocity (5) and (6) are listed in Tables I and II [12]-[32]. These include the impurity concentrations in Table I which were needed together with the sample length to obtain absolute absorption cross sections. The energy level positions obtained from the literature, and the average refractive index are given in Table II. (A listing of the references by material is presented as well.) It should be noted that, in some cases, where not all the energy levels of the electronic state were found, the calculated partition function was scaled to account for the missing levels. To scale the parameters, each partition function was multiplied by the number of levels expected divided by the number found.

The important spectroscopic parameters are listed in Table III, and the measured emission and absorption spectra are shown plotted on an absolute cross section scale in Figs. 2-4. The tabulated entries for the lifetime and cross section have been determined using the procedures described previously in Section II. In particular, the lifetimes reported in column 2 are the measured emission decay times. Column 3 is the calculated radiative lifetime. Column 4 is the value τ_s judged to be the most reasonable for calculating the emission cross section using (6): either column 2, column 3 or their average. The emission cross sections presented in Figs. 2-4 have been calculated from (6) using τ_s from column 4. The cross section value σ_{ext} reported in Table III corresponds to the selected extraction wavelength λ_{ext} where an asterisk

TABLE III
EMISSION PROPERTIES OF Yb^{3+} IN CRYSTAL HOSTS
(τ_{em} = measured emission lifetime; τ_{rad} = lifetime calculated by reciprocity; τ_s = average or selected lifetime; $\Delta E = E_{ZL} - h\nu$; β_{min} = minimum fractional population inversion required to have transparency at the extraction wavelength; σ_{ext} = emission cross section at extraction wavelength judged to be optimal; parentheses suggest greater uncertainty in the magnitude of the quantity.)

Host	τ_{em} (ms), Measured	τ_{rad} (ms) Calculated	τ_s (ms) Selected	λ_{ext} (nm)	ΔE (cm^{-1})	β_{min}	σ_{ext} (10^{-20} cm^2)
$LiYF_4$	2.16	2.27	2.21	1020	480	0.098	0.81
LaF_3	2.22	2.10	2.16	1009	353	0.113	0.36
SrF_2	9.72	(8.6)	9.2	1025	593	0.054	0.16
BaF_2	8.20	(7.8)	8.0	1024	578	0.058	0.14
$KCaF_3$	2.7	(4.0)	2.7	1031	(593)	0.070	0.22
KY_3F_{10}	2.08	1.66	1.87	1011	369	0.118	0.44
Rb_2NaYF_6	10.84	—	10.84	1012	(372)	0.140	0.10
BaY_2F_8	2.04	—	2.04	1018	(458)	0.097	0.67
Y_2SiO_5	1.04	—	1.04	1042	(617)	0.047	0.33
$Y_3Al_5O_{12}$	1.08	0.93	1.01	1031	628	0.055	2.03
$YAlO_3$	0.72	0.42[a]	0.42[a]	1014	353	0.141	1.31
$Ca_5(PO_4)_3F$	1.08	1.30	1.2	1043	603	0.046	5.90
$LuPO_4$	0.83	—	0.83	1011	349	0.160	0.53
$LiYO_2$	1.13	—	1.13	1020	(474)	0.090	0.56
$ScBO_3$	4.80	—	4.80	1022	(472)	0.091	0.19

[a]Only one of three polarizations accounted for.

marks the appropriate spectral features in Figs. 2–4. The reported ΔE is the difference in photon energy between the zero-line wavelength marked by an arrow in each figure and the extraction wavelength marked with an asterisk. The β_{min} are calculated with (12) and are listed in Table III.

A. Fluoride Hosts

Absorption and emission spectra for the two polarizations of uniaxial $LiYF_4$:Yb (YLF:Yb) have been obtained and the cross section plots are shown in Fig. 2. The energy levels were available from the literature [12] to calculate the partition functions and E_{ZL} values, as shown in Table II, and thus cross section determinations using the F–L and reciprocity methods were both carried out. The measured emission decay time τ_{em} and the lifetime calculated on the basis of reciprocity τ_{rad} agree very closely. The emission cross section has been calculated using the average of these two values $\tau = 2.21$ ms. The optimum cross section recorded in Table III for YLF is for light in which E is polarized parallel to the c axis; the extraction cross section σ_{ext} has a value of 0.81×10^{-20} cm^2 and a ΔE of 480 cm^{-1}.

The emission and absorption properties of LaF_3:Yb have been investigated. Emission cross section determinations were completed using both the reciprocity method [13] and the F–L equation. The measured emission decay and the lifetime evaluated by the reciprocity method are again in excellent agreement, as shown in Table III. Consequently, the average lifetime of 2.16 ms is utilized in the cross section determination by the F–L equation. Spectra of the two polarizations for both absorption and emission cross sections are plotted in Fig. 2. The emission cross section reported for LaF_3:Yb is for light polarized such that E is parallel to the c axis and is only 0.36×10^{-20} cm^2 and $\Delta E = 353$ cm^{-1}. In LaF_3, ΔE reflects the smallest ground state splitting we have observed throughout this study. The LaF_3 spectra are poorly articulated and appear primarily as a relatively unstructured broad band.

The host metal ions occupy a cubic eightfold coordinated site in crystals of SrF_2 and BaF_2. When trivalent ytterbium ions substitute for the divalent cations, however, the actual site symmetry is disrupted by the introduction of interstitial fluoride ions which provide the charge compensation. This is similar to the situation recently reported for Nd^{3+} in crystals with fluorite structure hosts [33]. The nature of the site symmetry depends on the impurity concentration, however, since at higher dopant levels, various impurity clusters begin to form. In order to more accurately determine the spectroscopic properties for the fluorite structure hosts, we have examined BaF_2 and SrF_2 crystals doped with different concentrations of Yb^{3+}.

At the lowest doping levels, the Yb^{3+} impurities occur as isolated ions distributed throughout the lattice. In these crystalline media, the environment serves to break the inversion symmetry via the introduction of interstitial fluorides for charge compensation. The compensating fluoride is relatively far from the Yb ion, however, since it occurs at the next-nearest interstitial site (along the [111] axis relative to the Yb ion). As a result, the transition strength introduced into the $4f$–$4f$ transitions by the charge compensation is small. With increasing impurity content, the Yb^{3+} centers begin to cluster. The inversion symmetry of the $4f$ wave function is disturbed to a much greater extent in the clusters. Significant changes in the spectra and absorption strengths bear this out. A series of absorption spectra were acquired with BaF_2 doped with 0.050,

0.093, 0.255, and 0.562 weight percent. Unique clustering features evident in the absorption spectra appear for samples at 0.255 weight percent and above, but not in the lower concentration samples. Consequently, the onset of clustering most likely occurs in the range of 0.1–0.2 weight percent ($1.68–3.36 \times 10^{19}$ Yb ions/cm^3). The same type of evaluation has also been done for SrF_2 with doping levels of 0.071, 0.152, 0.413, 0.768 weight percent. In this instance, the onset of clustering has been determined to lie between 0.2–0.4 weight percent ($2.95–5.90 \times 10^{19}$ Yb ions/cm^3).

To assess the emission cross section and lifetime of the isolated Yb^{3+} ion in the fluorite structure hosts that were not clustered, we have characterized the samples with low Yb content. Relatively long emission decay times have been measured for the isolated Yb^{3+} ion: BaF_2 with $\tau_{em} = 8.20$ ms and SrF_2 with 9.72 ms. The interstitial F^- is ineffective in inducing oscillator strength into the $4f$–$4f$ transitions, which is apparent from the low values of σ_{ext}, BaF_2 having a value of 0.14×10^{-20} and SrF_2 with 0.16×10^{-20} cm^2, as shown on the right-hand side (RHS) of Fig. 2. Although detailed energy level information was unavailable for ytterbium in SrF_2 or BaF_2, the isostructural compound CaF_2:Yb is available for a comparable analysis. The parenthetically reported entries in Table II for the BaF_2 and SrF_2 hosts are approximations which are derived from the CaF_2 data. Lifetimes of the highly doped samples were shorter, being on the order of 2 ms.

The sample of $KCaF_3$:Yb grown for this investigation was of poor optical quality. The compound is anisotropic, but $KCaF_3$ is derived from a slightly distorted perovskite structure and is nearly cubic in nature. Thus, as a result, an approximate treatment as an isotropic crystal was more practical. The middle, RHS of Fig. 2 displays the unpolarized absorption and emission cross sections for $KCaF_3$:Yb. Since the Yb ions are most likely incorporated at the divalent Ca site, some charge compensation is required to maintain electrical neutrality. The limited success growing this crystal and the low values of the measured cross sections, however, discouraged any further study of clustering and compensation effects.

The perovskite type structure of $KCaF_3$ is similar to compounds for which detailed spectroscopic data are available, including $KMgF_3$:Yb and $KZnF_3$:Yb [16]. Here, the divalent cations are coordinated by six fluorine ions, the supposed substitutional centers of the Yb^{3+} ion. In each of these analogs, Yb^{3+} emission properties arise from sites having both cubic and trigonal symmetry. The observed emission properties of Yb^{3+} in $KCaF_3$ suggest a single, noncubic site is preferentially occupied; a relatively short emission decay time of $\tau_{em} = 2.7$ ms has been measured, which is consistent with the lifetimes observed in most fluoride samples without centrosymmetric centers. On this basis, the energy levels of the Yb^{3+} in trigonal sites of the divalent metal for $KMgF_3$ and $KZnF_3$ have been employed to model the energy levels in $KCaF_3$. The approximated values in Tables II and III are the result of this procedure. The calculated radiative lifetime using the F–L equation was determined to be $\tau_{rad} = 4.0$ ms; this does not agree so favorably with the measured decay time of 2.7 ms. Due to the lack of better agreement between the two lifetimes and the uncertainty associated with the energy levels, the measured emission decay, rather than the average value, was selected for the calculation. Consequently, $\sigma_{ext} = 0.22 \times 10^{-20}$ cm^2 was obtained from the F–L equation at a $\Delta E \sim 593$ cm^{-1}. The zero-line energy is probably represented by the sharp line at 972 nm, although without additional data we cannot be sure that this suggestion is correct.

A crystal of the cubic compound KY_3F_{10}:Yb has been grown for our investigations. Large crystals of this material are rapidly obtained with little difficulty. The eightfold coordination of Y^{3+} by the fluorine atoms is arrayed in a crystal field of tetragonal symmetry. Detailed information of the energy levels of Yb^{3+} in this site have been reported [17], [18], and therefore the emission cross section is determined using both the F–L equation and the reciprocity method. Emission and absorption cross sections are presented in Fig. 2, lower right. The measured and calculated lifetimes are in good agreement, and therefore the averaged value of $\tau_s = 1.87$ ms has been utilized to determine the emission cross section. A cross section of $\sigma_{ext} = 0.44 \times 10^{-20}$ cm^2 for $\Delta E = 369$ cm^{-1} have been determined.

Another fluoride of interest is the cubic crystal of Rb_2NaYF_6:Yb [19], [20]. Fig. 2 contains the unpolarized emission and absorption cross sections of this material. The Y^{3+} site has perfect cubic symmetry and, as a result, the lifetime of the Yb^{3+} ion in such a crystal field is long, $\tau_{em} = 10.84$ ms. This emission lifetime is close to the value expected solely on the basis of the magnetic-dipole transition moment of 15 ms. The odd parity vibrational interactions are probably responsible for the residual difference from the measured lifetime. Energy levels for Yb^{3+} were unavailable for this compound so that the measured emission decay time was utilized as the input for the F–L equation, yielding the rather small emission cross section of $\sigma_{ext} = 0.10 \times 10^{-20}$ cm^2.

BaY_2F_8 is a monoclinic crystalline fluoride with a distorted eightfold site symmetry [21]. The biaxial nature requires three polarized spectra, each approximately along one of the dielectric axes. The absorption and emission cross sections are presented in Fig. 3. Insufficient energy level information is available to evaluate the emission cross section using the method of reciprocity, therefore the measured emission decay time has been utilized in the F–L equation to obtain σ_{em}. The optimum cross section in BaY_2F_8:Yb is observed for light polarized along z, although a similar cross section occurs for light polarized along y. The Yb^{3+} lifetime in BaY_2F_8:Yb is 2.04 ms and the extraction cross section is 0.67×10^{-20} cm^2.

B. Oxide Hosts

The RHS of Fig. 3 also portrays the emission and absorption cross section spectra for the biaxial crystal,

Y_2SiO_5:Yb (YOS:Yb). The three different spectra approximately correspond to the three principal polarizations of the dielectric axes. Two different sixfold coordinated Y^{3+} sites are present in the crystal structure and the Yb^{3+} ion may be situated at both of these [22]. The emission decay times were measured for Yb^{3+} in both sites, but site environments are sufficiently similar so that the nearly equal decay times were averaged and are reported as a single value, $\tau_{em} = 1.04$ ms. Presently, the energy level information required for the reciprocity method is unavailable, therefore the emission cross sections have been calculated using the measured decay time as the radiative lifetime in the F–L equation. The reported cross section value of $\sigma_{ext} = 0.33 \times 10^{-20}$ cm^2 is similar for each of the three polarizations.

A sample of cubic $Y_3Al_5O_{12}$:Yb (YAG:Yb) has been investigated and the unpolarized emission and absorption cross sections are shown in Fig. 4. Energy levels are known for Yb^{3+} in the distorted eightfold coordinated Y^{3+} site [23], [24], and this information is used to calculate the parameters reported in Table II. The method of reciprocity and the F–L equation have both been utilized and the calculated radiative lifetime was found to agree closely with the measured emission decay time (0.93 versus 1.08 ms). A determination of the emission cross section has been made using the average lifetime value $\tau_s = 1.01$ ms. This gave $\sigma_{ext} = 2.03 \times 10^{-20}$ cm^2 for $\Delta E = 628$ cm^{-1}. We note that several reports of the magnitude of emission cross section (1.8×10^{-20} cm^2 and 2.2×10^{-20} cm^2) are in accord with our results and stated accuracies [4]–[6].

The related yttrium aluminum oxide which has been investigated is the biaxial crystal $YAlO_3$:Yb (YALO:Yb). A full characterization of the emission and absorption spectra polarized along the principal dielectric axes was not obtainable from the unoriented sample available. However, measurements of several random polarizations were surveyed and no strong anisotropy was observed near 1.0 μm. Fig. 4 contains polarized absorption and corresponding emission cross section spectra. The energy levels of YALO have been studied [25]–[27] and parameters from the energy levels for the Yb^{3+} impurity are reported in Table II. Because the full polarization dependencies were not determined, an actual value for the radiative lifetime could not be calculated. The value of $\tau_{rad} = 0.42$ ms reported in Table III is the value obtained where a single polarized absorption and emission spectra are correlated by reciprocity. This value is used to determine the emission cross section value using the F–L equation. The measured emission decay time is 0.72 ms, and the emission cross section is 1.31×10^{-20} cm^2 for $\Delta E = 353$ cm^{-1}.

The spectral data of Yb-doped $Ca_5(PO_4)_3F$ (known as fluorapatite [28], [29], or FAP) are displayed in Fig. 4, lower left, for each of the two required polarizations of the crystal. These data represent the most remarkable finding of our study. The sparse spectra exhibit only the strong pump line at 905 nm, the emission line at 1043 nm, and the sharp features representing the zero-lines of two very similar Yb ions. The pronounced articulation of the spectra and a strong anisotropy, produce very large absorption and emission cross sections for light polarized along the c axis, 6.9×10^{-20} and 5.9×10^{-20} cm^2, respectively. In contrast, an emission spectrum polarized normal to c possesses a considerably lower cross section and may, as a result, lead to a mechanism by which amplified spontaneous emission (ASE) losses are reduced for some amplifier designs. The calculated and measured emission lifetimes of FAP:Yb are similar at 1.08 and 1.30 ms, and the $\Delta E = 603$ cm^{-1} value is suitably large to permit efficient extraction at 1043 nm.

The RHS of Fig. 4 contains the absorption and emission spectra of three more oxides: $LuPO_4$, $LiYO_2$, and $ScBO_3$ [30]–[32]. The orientational and polarization dependence of these crystals were not taken into account, consequently, the data on the RHS of Fig. 4 is only approximate. We utilized the measured decay time, along with the single unpolarized emission spectrum that was acquired, to calculate the emission cross section line shape and magnitude. The similar magnitudes of the absorption and emission cross sections evidenced in Fig. 4, however, suggest that the resulting systematic error is probably no greater than 50%.

The measured emission decay times are 0.83 and 1.13 ms for $LuPO_4$ and $LiYO_2$, respectively. Although the spectra are only approximate, we can observe that the Yb^{3+} crystal field splitting is about twice as large in $LiYO_2$, as compared to $LuPO_4$ (measured by the overall width of the spectra). The low crystal field splitting in $LuPO_4$ makes β_{min} large, and the broad emission lines of $LiYO_2$:Yb yield low peak cross sections. Accordingly, neither $LuPO_4$ or $LiYO_2$ are particularly interesting for laser applications. The spectra of $ScBO_3$:Yb appear in the lowest frame, where it is apparent that the magnitudes of the cross sections are very low. The weak transition strength is also reflected in the long emission lifetime of 4.80 ms. $ScBO_3$ crystallizes in the calcite structure where the Yb^{3+} enters the centrosymmetric Sc-site, thereby giving rise to the low cross sections and long lifetime.

V. Discussion

Yb^{3+} exhibits a significant range of emission cross sections, 0.1 to 5.9×10^{-20} cm^2, and lifetime values of 0.7–10.8 ms, which suggest numerous factors must impact these properties. For example, the materials with the longest lifetimes, 5–11 ms, including SrF_2, BaF_2, Rb_2NaYF_6, and $ScBO_3$, all possess nearly centrosymmetric sites into which the Yb ion is incorporated. On the other hand, most of the fluorides having noncentrosymmetric substitutional sites, including $LiYF_4$, LaF_3, KY_3F_{10}, and BaY_2F_8, give lifetimes of 2.0–2.2 ms, and oxides with the noncentrosymmetric sites (Y_2SiO_5, $Y_3Al_5O_{12}$, $YAlO_3$, $Ca_5(PO_4)_3F$, $LuPO_4$, and $LiYO_2$) have decay times of 0.7–1.1 ms. The consistency of these values, although somewhat surprising, provides a useful guide by which to think about Yb lifetimes in crystalline media.

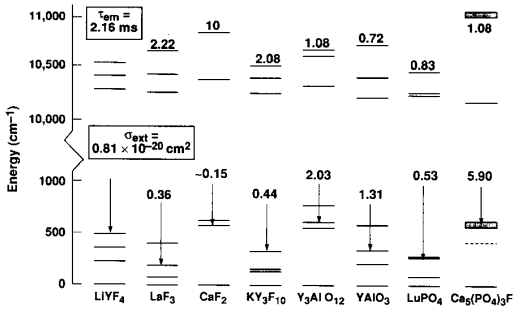

Fig. 5. The important spectroscopic properties, of Yb^{3+} in the designated crystal hosts, and the energy levels of the ground- and excited-states are presented. The emission cross section at the selected extraction wavelength σ_{ext} is noted, as is the measured emission lifetime τ_{em}. The termination point of the downward-facing arrow gives the value of ΔE at the extraction wavelength.

TABLE IV
CALCULATED LASER PROPERTIES OF Yb-DOPED CRYSTALS AT THE SELECTED PUMP AND EXTRACTION WAVELENGTHS, λ_{pump} AND λ_{ext}
(I_{sat} = pump saturation intensity at λ_{pump}; I_{min} = minimum pump intensity required to achieve transparency at λ_{ext}; σ_{ext} = emission cross section at λ_{ext}; parentheses reflect uncertainty in the value of the quantity)

Host	λ_{pump} (nm)	I_{sat} (kW/cm^2)	I_{min} (kW/cm^2)	λ_{ext} (nm)	σ_{ext} (10^{-20} cm^2)
$LiYF_4$	962	10.2	1.00	1020	0.81
LaF_3	975	16.9	1.90	1009	0.36
SrF_2	967	6.8	0.37	1025	0.16
BaF_2	967	6.1	0.36	1024	0.14
$KCaF_3$	973	5.0	(0.35)	1031	0.22
KY_3F_{10}	976	13.3	1.57	1011	0.44
Rb_2NaYF_6	962	14.7	(2.05)	1012	0.10
BaY_2F_8	961	13.2	(1.28)	1018	0.67
Y_2SiO_5	979	8.5	(0.40)	1042	0.33
$Y_3Al_5O_{12}$	942	27.9	1.53	1031	2.03
$YAlO_3$	962	31.9	4.50	1014	1.31
$Ca_5(PO_4)_3F$	905	2.86	0.132	1043	5.90
$LuPO_4$	975	18.6	2.98	1011	0.53
$LiYO_2$	908	16.7	(1.50)	1020	0.56
$ScBO_3$	966	18.6	(1.70)	1022	0.19

The emission cross sections corresponding to the extraction wavelengths vary in a much less consistent manner. For instance, for the fluorides with lifetimes near 2 ms, σ_{ext} values of (0.36–0.81) $\times$ 10^{-20} cm^2 are obtained, and the oxide systems with τ_{em} = 0.7–1.1 ms give σ_{ext} = (0.33–5.9) $\times$ 10^{-20} cm^2. The media with centrosymmetric sites do exhibit the lowest cross sections, as expected.

Besides the radiative emission lifetime, the other crucial issue that impacts the extraction cross section is the emission line shape. An emission spectrum characterized by a sharp peak at a long wavelength is construed to have a favorable line shape. The examples of Yb-doped crystals characterized by particularly favorable line shapes are SrF_2, $Y_3Al_5O_{12}$ and $Ca_5(PO_4)_3F$, see Figs. 2–4. The fundamental basis for the existence of the sharp long-wavelength feature may be understood from the energy levels sketched in Fig. 5. Here it is apparent that the $^2F_{7/2}$ ground state possesses a substantial gap between the terminal laser level and the next lowest crystal field component for these three Yb-doped crystals (the CaF_2 energy levels are representative of SrF_2). The effect of this energy gap may be to reduce the rate of phonon relaxation, and thereby give rise to sharper spectral features. In the case of SrF_2:Yb, however, the emission cross section is low, by virtue of the centrosymmetric site and the long emission lifetime. The YAG:Yb spectrum, on the other hand, has a high emission cross section of 2.0 $\times$ 10^{-20} cm^2. Although there remains some uncertainty as to the exact ground state energy levels of Yb in $Ca_5(PO_4)_3F$ (note the dashed line in Fig. 5), it is apparent that the Yb energy levels and the host lattice have conspired to provide sharp spectral features in this case.

The largest cross section among the fluorides is seen in $LiYF_4$:Yb, in spite of the unfavorable spacing of the energy levels displayed in Fig. 5. The large σ_{ext} value of $LiYF_4$ follows from the strongly polarized emission evidenced by this crystal. Here, the emission intensity is π-polarized so that all of the cross section is, in effect, "concentrated" into a particular orientation. It is noteworthy that $Ca_5(PO_4)_3F$ (FAP) possesses both the orientational advantage (since it is strongly π-polarized, see

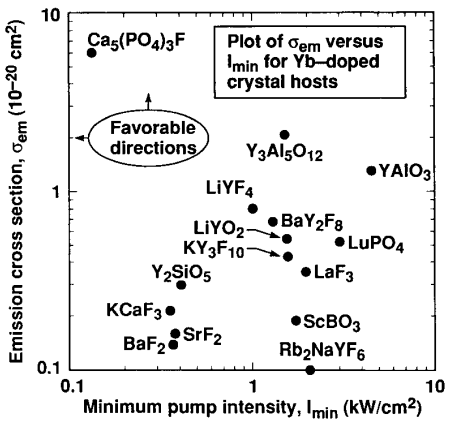

Fig. 6. A log plot of emission cross section σ_{em} versus minimum pump intensity I_{min} for the selected extraction wavelength. The σ_{em} values for each host correspond to σ_{ext} in Table III and are judged to be near the optimum for rapid energy extraction. The emission cross section describes the gain that will be available for a given inversion density and therefore higher σ_{em} values are desirable. I_{min} is the minimum pump power required for each crystal to reach threshold or the intensity required to pump the medium to an inversion density exhibiting no net loss at λ_{ext}. Low I_{min} values are desirable. The arrows mark the preferred directions and reveal that $Ca_5(PO_4)_3F$: Yb is unique because of its highly favorable parameters.

Fig. 4), and the favorable energy level structure (giving the sharp spectral features).

The overall suitability of an Yb-doped crystal for laser applications depends on many and varied factors. The two main issues regarding spectral properties, concern the ease of pumping the laser material, and that of extracting the stored energy. Table IV contains a listing of the most effective pump wavelength λ_{pump} for each of the crystals. On the basis of the observed absorption cross sections from Figs. 2–4, and the emission lifetimes of Table III, the pump saturation intensities I_{sat} have been calculated, as well as the minimum pump intensities required to reach threshold I_{min} [see Section III-D, (10)–(13)]. I_{min} may be regarded as a figure-of-merit describing the intensity required to pump the medium to a suitable inversion density. Also reported in Table IV are the emission cross sections σ_{ext} at the selected extraction wavelengths λ_{ext}. The σ_{ext} is, of course, the appropriate parameter needed to describe the gain that will be available for a given inversion density.

We suggest that the I_{min} and σ_{ext} parameters together provide a good spectroscopic measure of the overall usefulness of the laser medium. The I_{min} and σ_{ext} values of each crystal are plotted in Fig. 6; it is generally desirable for σ_{ext} to be as large as possible and for I_{min} to be small. This criterion serves to both minimize the threshold for an Yb-laser material engaged in an oscillator-type configuration, and also to offer the best short-pulse amplification properties. It is apparent from Fig. 6 that Yb in $Ca_5(PO_4)_3F$ (FAP) is by far the most favorable material when judged on this basis. It is interesting that FAP: Yb appears to uniquely occupy a superior domain in parameter space than do the other fourteen materials plotted in Fig. 6. On the basis of this analysis, an Yb: FAP laser, pumped at 905 nm using a Ti: Al_2O_3 laser, has been demonstrated and characterized. We have found that the observed laser performance agrees with the spectroscopic properties reported here. These laser results and the bulk optical, thermal and mechanical properties of the host will be described in a future publication.

VI. Conclusion

The absorption and emission cross sections of the $^2F_{7/2}$–$^2F_{5/2}$ transition and the upper laser level lifetimes of the Yb^{3+} ion have been determined for 15 hosts. The emission cross sections were determined by two methods. The first, based on the principle of reciprocity, requires the absorption spectrum, the Yb^{3+} concentration and a detailed knowledge of the energy levels. The second utilizes the classic relationship between spontaneous and stimulated emission rates (Füchtbauer–Ladenburg formula) for which the emission spectra, the refractive index and the measured lifetime are required. The emission cross section of the reciprocity method was then employed in the Füchtbauer–Ladenburg equation, and a separate value for the radiative lifetime was calculated. The calculated and measured lifetimes have been compared, and the agreement is good between the two, typically within 20%.

The measured spectroscopic properties of the Yb^{3+} ion have been studied in various hosts, focusing on their adequacy for diode-pumping the Yb laser material. From our analysis, the more useful diode-pumped Yb laser material, operating in a short pulse extraction mode, will require σ_{ext} magnitudes of $>10^{-20}$ cm^2 and ground state splittings of the terminal laser level of $\Delta E > 400$ cm^{-1}. With each of the crystal field environments the Yb^{3+} ion encountered, large ground state splittings were observed, and in fact the $\Delta E > 400$ cm^{-1} criterion was satisfied in most cases. On the other hand, the emission cross sections at the extraction wavelength were less than satisfactory for most hosts. In particular, in nearly cubic crystal field environments where the Yb^{3+} emissions were longer lived, the cross sections were very low. In SrF_2, BaF_2, Rb_2NaYF_6, and $ScBO_3$, all with centrosymmetric sites, $\sigma_{ext} < 0.2 \times 10^{-20}$ cm^2 were measured. Useful emission cross sections were observed for some of the materials exhibiting a favorable emission line shape characterized by a sharp peak at a long wavelength, as is the case for $Y_3Al_5O_{12}$ and $Ca_5(PO_4)_3F$, for example. We have discussed this situation relative to the Yb^{3+} energy levels, where, for large energy gaps between the terminal laser level and lowest crystal field component, reduced rates of phonon relaxation might be expected to give rise to sharper spectral features. Among the 15 hosts we have studied, the Yb^{3+} energy levels and the host lattice have conspired to provide adequate emission cross sections only in $Y_3Al_5O_{12}$ and $Ca_5(PO_4)_3F$.

The spectral properties relevant to the predicted laser performance establish the ease of pumping the laser material and that of extracting the stored energy. We have suggested two parameters I_{min} and σ_{ext}, taken together effectively, describe the usefulness of the laser medium.

Since it is desirable to have higher values of σ_{ext} and lower values of I_{min}, Yb^{3+} in $Ca_5(PO_4)_3F$ is judged to be unique in its occupation of a favorable sector of this parameter space.

Acknowledgment

We wish to acknowledge the skilled efforts of many at Lawrence Livermore National Laboratory. In particular, E. Prochnow and R. Vallene fabricated and polished samples for our use, T. Duewer and C. Otto measured the Yb concentrations, and J. Tassano provided technical support in the crystal growth operations. We also wish to thank M. Weber for the loan of several crystals. T. Pollak of Sanders Associates, R. Sparrow of Optovac, L. Boatner of Oak Ridge National Laboratory, and N. Edelstein of Lawrence Berkeley Laboratory are also thanked for the crystals that they have supplied us.

References

[1] R. M. Kolbas, N. G. Anderson, W. D. Laidig, Y. Sin, Y. C. Lo, K. Y. Hsieh, and Y. J. Yang, "Strained-layer InGaAs-GaAs-AlGaAs photopumped and current injection lasers," *IEEE J. Quantum Electron.*, vol. 24, pp. 1605-1613, Aug. 1988.

[2] D. P. Bour, D. B. Gilbert, K. B. Fabian, J. P. Bednarz, and M. Ettenberg, "Low degradation rate in strained InGaAs/AlGaAs single quantum well lasers," *IEEE Photon. Technol. Lett.*, vol. 2, pp. 173-174, Mar. 1990.

[3] For numerous examples, see P. Moulton, "Paramagnetic ion lasers," in *Handbook of Laser Science and Technology*, M. J. Weber, Ed. Boca Raton, FL: CRC, 1983, p. 211.

[4] A. R. Reinberg, L. A. Riseberg, R. M. Brown, R. W. Wacker, and W. C. Holton, "GaAs:Si LED pumped Yb-doped YAG laser," *Appl. Phys. Lett.*, vol. 19, p. 11, 1971.

[5] P. Lacovara, H. K. Choi, C. A. Wang, R. L. Aggarwal, and T. Y. Fan, "Room-temperature diode-pumped Yb:YAG laser," *Opt Lett.*, vol. 16, no. 14, pp. 1089-1091, 1991.

[6] W. F. Krupke and L. L. Chase, "Ground-state depleted solid-state lasers: principles, characteristics and scaling," *Opt. Quantum Electron.*, vol. 22, pp. S1-S22, 1990.

[7] D. E. McCumber, "Einstein relations connecting broadband emission and absorption spectra," *Phys. Rev.*, vol. 136, pp. A954-A957, 1964.

[8] S. A. Payne, L. L. Chase, L. K. Smith, W. L. Kway, and W. F. Krupke, "Infrared cross section measurements for crystals doped with Er^{3+}, Tm^{3+} and Ho^{3+}," *IEEE J. Quantum Electron.*, vol. 28, pp. 2619-2630, 1992.

[9] P. F. Moulton, "Spectroscopic and laser characteristics of $Ti:Al_2O_3$," *J. Opt. Soc. Amer.*, vol. B3, pp. 125-133, 1986.

[10] W. Koechner, *Solid-State Laser Engineering*. New York: Springer, 1986, p. 17.

[11] W. T. Carnall, P. R. Fields and B. G. Wybourne, "Spectral intensities of the trivalent lanthanides and actinides in solution. I. Pr^{3+}, Nd^{3+}, Er^{3+}, Tm^{3+}, and Yb^{3+}," *J. Chem. Phys.*, vol. 42, no. 11, pp. 3797-3806, 1965.

[12] C. A. Morrison and R. P. Leavitt, "Spectroscopic properties of triply ionized lanthanides in transparent host crystals," in *Handbook of Physics and Chemistry of Rare Earths*, vol. 5, K. A. Gschneidner, Jr. and L. Eyring, Eds. New York: North-Holland, 1989.

[13] W. T. Carnall, G. L. Goodman, K. Rajnak, and R. S. Rana, "A systematic analysis of the spectra of the lanthanides doped into single crystal LaF_3," *J. Chem. Phys.*, vol. 90, no. 7, pp. 3443-3457, 1989.

[14] Yu. K. Voron'ko, V. V. Osiko, and I. A. Shcherbakov, "Optical centers and the interaction of Yb^{3+} ions in cubic fluorite crystals," *Sov. Phys.-JETP*, vol. 29, no. 1, pp. 86-90, 1969.

[15] J. Kirton and S. D. McLaughlin, "Correlation of electron paramagnetic resonance and optical-absorption spectra of $CaF_2:Yb^{3+}$," *Phys. Rev.* vol. 155, no. 2, pp. 279-284, 1967.

[16] A. A. Antipin, A. V. Vinokurov, M. P. Davydova, S. L. Korableva, A. L. Stolov, and A. A. Fedii, "Optical spectra, EPR, and spin-lattice relaxation of Yb^{3+} ions in crystals having perovskite-type structure," *Phys. Stat. Sol. (b)*, vol. 81, pp. 287-293, 1977.

[17] R. Yu. Abdulsabirov, A. V. Vinokurov, V. A. Ivanshin, I. N. Kurkin, E. A. Pudovik, A. L. Stolov, and Sh. I. Yagudin, "Optical spectra and spin lattice relaxation of rare-earth ions in KY_3F_{10} crystals," *Opt. Spectrosc. (USSR)*, vol. 63, no. 1, pp. 55-58, 1987.

[18] R. Yu. Abdulsabirov, M. A. Dubinskii, B. N. Kazakov, N. I. Silkin, and Sh. I. Yagudin, "New fluoride laser matrix," *Sov. Phys. Crystallogr.*, vol. 32, no. 4, pp. 559-562, 1987.

[19] F. S. Richardson, M. F. Reid, J. J. Dallara, and R. D. Smith, "Energy levels of lanthanide ions in the cubic $Cs_2NaLnCl_6$ and $Cs_2NaYCl_6:Ln^{3+}$ (doped) systems," *J. Chem. Phys.*, vol. 83, no. 8, pp. 3813-3830, 1985.

[20] P. A. Tanner, "Electronic spectra of Yb^{3+} in elpasolite lattices," *Molec. Phys.*, vol. 58, no. 2, pp. 317-328, 1986.

[21] A. A. Kaminskii, B. P. Sobolev, S. E. Sarkisov, G. A. Denisenko, V. V. Ryabchenko, V. A. Fedorov, and T. V. Uvarova, "Physicochemical aspects of the preparation, spectroscopy, and stimulated emission of single crystals of $BaLn_2F_8:Ln^{3+}$," *Inorg. Mat. (USSR)*, vol. 20, pp. 402-416, 1982.

[22] R. Beach, M. Shinn, L. Davis, R. Solarz and W. Krupke, "Optical absorption and stimulated emission of neodymium in yttrium orthosilicate," *IEEE J. Quantum Electron.*, vol. 26, pp. 1405-1412, Aug. 1990.

[23] Kh. S. Bagdasarov, G. A. Bogomolova, D. N. Vylegzhanin, A. A. Kaminskii, A. M. Kevorkov, A. G. Petrosyan, and A. M. Prokhorov, "Luminescence and stimulated emission of Yb^{3+} ions in aluminum garnets," *Sov. Phys. Dokl.*, vol. 19, no. 6, pp. 358-359, 1974.

[24] G. A. Bogomolova, D. N. Vylegzhanin, and A. A. Kaminskii, "Spectral and lasing investigations of garnets with Yb^{3+} ions," *Sov. Phys.-JETP*, vol. 42, no. 3, pp. 440-446, 1976.

[25] M. J. Weber, T. E. Varitimos and B. H. Matsinger, "Optical intensities of rare-earth ions in yttrium orthoaluminate," *Phys. Rev. B*, vol. 8, no. 7, pp. 47-53, 1973.

[26] Yu. E. Perlin, A. A. Kaminskii, V. N. Enakii, and D. N. Vylegzhanin, "Electron-phonon resonances in the spectrum of a rare-earth impurity ion," *JETP Lett.*, vol. 30, no. 7, pp. 398-401, 1979.

[27] M. J. Weber, "Optical properties of Yb^{3+} and $Nd^{3+} - Yb^{3+}$ energy transfer in $YAlO_3$," *Phys. Rev. B*, vol. 4, no. 9, pp. 3153-3159, 1971.

[28] B. S. Gorobets, "On the luminescence of fluorapatite activated by rare-earth elements," *Opt. Spectrosc.*, vol. 25, pp. 154-155, 1968.

[29] A. M. Morozov, L. G. Morozova, A. K. Trefimov and P. P. Feofilov, "Spectral and luminescent characteristics of fluorapatite single crystals activated by rare earth ions," *Opt. Spectrosc.*, vol. 29, pp. 590-594, 1971.

[30] P. C. Becker, T. Hayhurst, G. Shalimoff, J. G. Conway, N. Edelstein, L. A. Boatner and M. M. Abraham, "Crystal field analysis of Tm^{3+} and Yb^{3+} in YPO_4 and $LuPO_4$," *J. Chem. Phys.*, vol. 81, no. 7, pp. 2872-2878, 1984.

[31] V. A. Antonov, P. A. Arsenev, Sh. A. Vanhidov, E. M. Ibragimova and D. S. Petrova, "Spectroscopic properties of neodymium ions in $LiYO_2$ monocrystals," *Phys. Stat. Sol. (a)*, vol. 41, pp. 45-50, 1977.

[32] B. H. T. Chai, M. Long, R. C. Morris, and S. T. Lai, "Crystal growth of $ScBO_3:Cr^{2+}$—a new near-IR tunable laser crystal," in *Tunable Solid State Lasers II*, A. B. Budgor, L. Esterowitz, and L. G. DeShazer, Eds. New York: Springer-Verlag, 1986.

[33] S. A. Payne, J. A. Caird, L. L. Chase, L. K. Smith, N. D. Nielsen, W. F. Krupke, "Spectroscopy and gain measurements of Nd^{3+} in SrF_2 and other fluorite-structure hosts," *J. Opt. Soc. Amer. B*, vol. 8, no. 4, pp. 726-740, 1991.

Laura Davis DeLoach, for a photograph and biography, see p. 507 of the February 1993 issue of this JOURNAL.

Stephen A. Payne was born in the Bronx, NY, on October 24, 1957. He received the B.S. degree in chemistry from the State University of New York at Binghamton in 1978 and the Ph.D. Degree in chemistry from Princeton University, Princeton, NJ, in 1983.

From 1983 to 1985 he was a post-Doctoral Fellow at the University of Pennsylvania, Philadelphia. Presently, he is a physicist and group leader at Lawrence Livermore National Laboratory, Livermore, CA, where he is conducting research on the optical properties of solid-state laser materials. He has participated in identifying several new laser materials, such as Cr:LiSAF and has been involved in the elucidation of the fundamental mechanisms operative in solid-state media. His previous research includes two-photon spectroscopy of ions-in-crystals, and measurements of coherent anti-Stokes Raman scattering using picosecond lasers.

Dr. Payne is a member of the American Physical Society and the Optical Society of America.

L. L. Chase, photograph and biography not available at the time of publication.

Larry K. Smith was born in Dallas, TX, in May 1957. He attended Texas State Technical Institute where he graduated in 1980 with an associate degree in laser electrooptics.

He then went to work for Bendix Field Engineering at Lawrence Livermore National Laboratory as a Laser and Target Alignment Technician on the Argus, Shiva, and Novette laser systems. Since 1984 he has been with LLNL working in the Advanced Laser Materials Group, where he has been responsible for characterizing and lasing new materials.

Wayne L. Kway received the B.S. degree in chemistry from the University of California, Berkeley.

He then served in the semiconductor industry for nine years as an engineer in silicon crystal growth development. He then joined the Center for Materials Research, Stanford University, as a research engineer in the Crystal Sciences Division. In this capacity, he spent 16 years in the development and perfection of single crystal and fiber materials for electrooptics, acoustooptics, and laser research. Since 1986, he has been serving as a chemist at LLNL in the Advanced Laser Materials Group, and is currently conducting crystal growth development for advanced solid-state laser applications.

Mr. Kway is a member of the American Association for Crystal Growth and a member of the Northern California Growers Association.

William F. Krupke received the B.S. degree in physics from Rensselaer Polytechnic Institute, Troy, NY, and the M.A. and Ph.D. degrees, also in physics, from the University of California, Los Angeles.

He is currently Deputy Associate Director of the Laser Directorate at the Lawrence Livermore National Laboratory (LLNL), Livermore, CA. Reporting to the Associate Director, he advises on top-level scientific, technical, and programmatic aspects of programs in the Laser Directorate. Core national programs include the Atomic Vapor Laser Isotope Separation (AVLIS) and the Inertial Confinement Fusion (ICF) programs of the U.S. Department of Energy, operating at $250 million/year. In addition to these executive responsibilities, he provides working scientific and technical leadership for the development of advanced applications programs in field of lasers and electrooptics. Current research and development efforts are centered on development of semiconductor laser diode arrays, novel solid-state laser materials, and high-power solid-state laser devices and systems. During his 18 years at LLNL, he served eight years as a technical line manager for the design and development of the 10 kJ SHIVA Nd:glass ICF Laser System, and for the design, development, and assessment of excimer, copper vapor, liquid dye, and solid-state lasers for AVLIS and ICF applications. He also served a year as Chief Scientist for the Laser Directorate before assuming his present position. Prior to joining LLNL, he held Technical Staff and Associate Department manager positions at the Laser Division, Hughes Aircraft Company. He performed original scientific work, and subsequently managed programs in the areas of microwave magnetic devices, solid-state laser materials and devices, nonlinear optical devices, carbon dioxide electric and gas dynamic lasers, and chemical lasers. He also spent several years as a technical staff member of the Aerospace Corporation and Minneapolis Honeywell Company where he performed the original research on solid-state lasers and optical radar. He has been granted seven patents and has published over 30 papers in scientific journals on lasers and electrooptics. He is an internationally recognized expert on solid-state laser materials and devices.

Dr. Krupke is a member of the American Physical Society and the Optical Society of America.